*Environmental Health Perspectives*
*Vol. 79, pp. 151-157, 1989*

# Regional Deposition of Inhaled Fog Droplets: Preliminary Observations

## by Stephen M. Bowes, III,* Beth L. Laube,* Jonathan M. Links,* and Robert Frank*

**The regional deposition of a monodisperse 10-μm mass median aerodynamic diameter fog was studied in four healthy adult male nonsmokers. The fog was radiolabeled with technetium-99m sulfur colloid to enable detection by an Anger camera of deposited activity in the following regions of the respiratory tract: oropharynx, larynx, trachea, and intrapulmonary airways. Intrapulmonary deposition was further analyzed by computer with inner, intermediate, and outer zones, and within apical, intermediate and basal zones of the right lung. The radiolabeled aerosol was inhaled by mouth through a face-mask with the nasal airway occluded. Respiratory frequency, tidal volume, and jaw position were controlled and were commensurate with the oral component of oronasal breathing during moderate exercise. Deposition in the larynx, trachea, and intrapulmonary airways was a function of the scrubbing efficiency of the oropharynx, which differed substantially among subjects, and ranged from 72 to 99%. The density of the aerosol deposit in the larynx probably exceeded that of any of the subdivisions of the tracheobronchial tree and lung. Within the lung, deposition favored the inner zone (assumed to contain the larger airways) over the outer zone (assumed to be dominated by smaller airways and alveoli). Intrapulmonary aerosol distribution in an elderly subject with borderline evidence of airway obstruction differed from that observed in younger subjects. The possible consequences of altered lung elastic recoil, as may occur with aging, for regional dosimetry is discussed.**

## Introduction

Ambient fog can be strongly acidic. Most of this acidity is attributable to sulfuric ($H_2SO_4$) and nitric ($HNO_3$) acids, although volatile organic acids may play a contributory role (*1*). The relative contributions of sulfate ($SO_4$) and nitrate ($NO_3$) to fog acidity varies geographically (Table 1). The $NO_3$:$SO_4$ ratio is generally less than 1 in the northeastern and midwestern United States. The reverse is true in the Los Angeles Basin, where $NO_3$ is the dominant species.

Fog is highly unstable. The water content of fog droplets, hence their size and pH, is subject to continual spatial and temporal variation. When water vapor condenses on preexisting nuclei and fog begins to form, the droplets are relatively small and their pH is low (Table 2). As water vapor condensation continues, the droplets increase in size and pH. Later, when evaporation begins, the process is reversed and the fog dissipates. In a mature fog, droplet growth and shrinkage may occur continuously as the air temperature fluctuates.

The degree to which acidic fog penetrates beyond the oropharynx should influence its potential hazard to health. Our objective was to characterize regional deposition within the human respiratory tract of monodisperse fog droplets inhaled by mouth at a ventilatory rate commensurate with moderate exercise. We selected a 10-μm mass median aerodynamic diameter (MMAD) aerosol as one more likely to typify the early and late stages of fog, when pH is relatively low. We used a monodisperse aerosol to better compare the results with both predictive deposition models and empirical studies, which generally used monodisperse aerosols. Preliminary observations on four healthy male adults are presented and the results should therefore be regarded as tentative.

## Methods

The four volunteers in this study were healthy adult male nonsmokers. The timed, forced vital capacity (body temperature, pressure, saturated) was measured

*Human Exposure Assessment Laboratory of the Department of Environmental Health Sciences, The Johns Hopkins School of Hygiene and Public Health, and Division of Clinical Immunology and Department of Radiology, The Johns Hopkins School of Medicine, Baltimore, MD 21205.

**Table 1. Chemical and physical properties of acid fog.**

| Location | pH | $NO_3/SO_4$ | Liquid water content, $g/m^3$ | $[H^+]$ as equivalent | |
|---|---|---|---|---|---|
| | | | | $[H_2SO_4]$, $\mu g/m^3$ | $[HNO_3]$, $\mu g/m^3$ |
| Bar Harbor, ME (*30*) | 2.90 | 0.3 | — | — | — |
| Los Angeles, CA (*31*) | 2.66 | 2.2 | 0.14 | 15 | 19 |
| | 2.16 | 6.1 | 0.11 | 37 | 48 |

**Table 2. Fog droplet average diameter (*32*).**

| Stage | Size, μm |
|---|---|
| Fog formation | 8–12 |
| Mature fog | 10–20 |
| Fog dissipation | 8–16 |

with an 8-L survey spirometer (Warren E. Collins, Inc.) with the subjects seated. The test was performed and recorded as recommended by the American Thoracic Society (*2*). The experimental protocol was as follows. After the pulmonary function tests, a xenon ventilation image was obtained on the subject to identify lung borders. Next, the subject inhaled a 10-μm aerosol labeled with technetium-99m ($^{99m}Tc$) sulfur colloid during controlled breathing. After rinsing the activity from the oral airway, the subject stood before an Anger camera for imaging of the lateral skull and lungs. The images were analyzed by computer to evaluate the regional distribution of the radioaerosol. Each step is described in detail below.

## Ventilation Image

A ventilation image was obtained to identify lung borders and enable subsequent matching of regional ventilation and aerosol distribution. The subject inhaled xenon-133 gas through a face mask while standing in front of a large-field Anger camera (Technicare model 110) equipped with an all-purpose parallel hole collimator. Subjects breathed the radiogas for 90 sec to promote penetration throughout the lung. A 600,000 count image of the anterior lung was acquired by computer (Technicare model 450) in a 256 × 256 picture element (pixel) matrix and stored on magnetic tape.

## Aerosol Generation and Administration

The inhalation method is shown schematically in Figure 1. A 10-μm MMAD monodisperse aerosol was generated from a sterile suspension of technetium-99m sulfur colloid in saline with a modified spinning top aerosol generator (*3,4*). The aerosol was diluted with humidified air (200 Lpm, 25°C, 98–99% relative humidity) and flowed through flexible tubing to a facemask held by the subject against his face. The mask was designed to separate oral and nasal airflow and to minimize distortion of the oral and nasal airways. The particle size distribution was measured at the facemask using a factory-calibrated aerodynamic particle sizer (TSI, Inc.). A typical particle size distribution is presented in Figure 2.

## Breathing Pattern and Oral Airway Configuration

With the face mask in position, and prior to the administration of the radioactive aerosol, the subject breathed clean air by nose. Inhalation of radioaerosol began by occluding the nose port, and the subject breathed the radioaerosol entirely by mouth. Respiratory frequency and tidal volume were fixed at 24 breaths/min and 1 L, respectively. These levels are commensurate with the oral component of oronasal breathing during moderate exercise (*5*). Respiratory frequency was controlled with the aid of a metronome. Tidal volume was measured with an inductive plethysmograph (Respitrace, Ambulatory Monitoring, Inc.). The signal from the plethysmograph was recorded (Model 7D Polygraph, Grass Instruments, Inc.) and displayed on an oscilloscope (2215A, Tektronix,

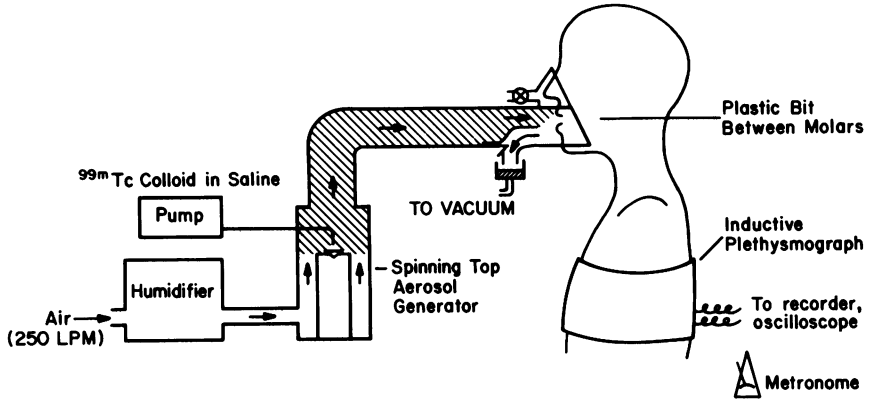


FIGURE 1. Monodisperse aerosol generator and inhalation apparatus showing valve to nasal compartment of face mask closed off. See text for details.

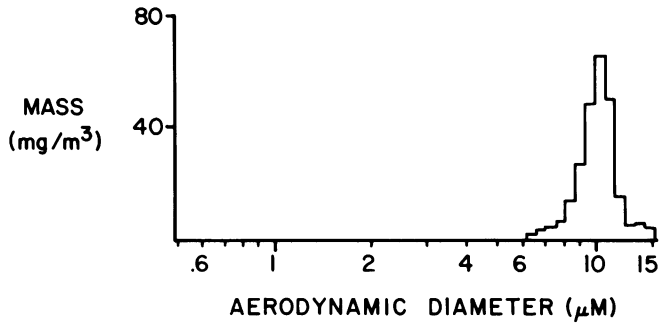


FIGURE 2. Distribution of particle mass (mg/m³) as a function of aerodynamic particle diameter (μm) from the spinning top generator measured at the face mask. Droplets consist of $^{99m}$Tc sulfur colloid in isotonic saline. MMAD = 10.3 μm, geometric SD = 1.1. Range of particle size in the four experiments was 9.6 to 10.3 μm, MMAD; geometric SD in all studies was 1.1.

Inc.). The subject used the oscilloscopic display to control tidal volume. The position of the jaw was fixed by means of a plastic bit (1 cm long, 3–5 mm diameter) placed between the molars. This placement was intended to reproduce the vertical distance (1–2 mm) between anterior incisors observed during earlier treadmill exercise of the subject when his ventilation level was about 45 to 50 L/min.

## Radioaerosol Inhalation

Inhalation of the radioaerosol lasted 4 to 10 min depending on the concentration of radioactivity in the aerosol. The concentration of radioactivity in the aerosol was measured prior to inhalation by drawing a known volume of aerosol through a filter and counting the filter activity. Immediately following radioaerosol inhalation, the subject gargled and rinsed his mouth several times with water, then swallowed water to clear esophageal activity to the stomach. The rinse was collected in a container for subsequent counting. Total inhaled activity ranged from 82 to 534 microcuries (μCi).

## Aerosol Deposition Imaging

Following the mouth rinse, the subject stood in front of an Anger camera for imaging of the left lateral skull and anterior and posterior chest. The left lateral skull image was used to assess oropharyngeal and laryngeal deposition. The chest image was used to assess tracheal and intrapulmonary deposition and stomach activity. The Anger camera images were acquired in a 256 × 256 pixel matrix and stored on magnetic tape for analysis. Each imaging procedure lasted from 2.5 to 20 min depending upon the total amount of radioactivity deposited in the subject.

Images of the left lateral skull and anterior and posterior chest were processed in a 64 × 64 pixel matrix using a computer (Informatek SIMIS). Activity detected in the lungs, stomach, and trachea was adjusted to compensate for camera sensitivity and tissue attenuation based on the conversion equation of Macey and Marshall (*6*). Activity detected in the oropharynx and larynx was adjusted by dividing detected activity by left lateral skull sensitivity. Left lateral skull sensitivity was determined by counting a known amount of $^{99m}$Tc (5–10 μCi), which was placed in the back of the subject's mouth as a point source.

Total aerosol deposition was determined from the sum of activity in each region of interest (oropharynx, larynx, trachea, intrapulmonary region, and stomach). For all analyses of anatomical aerosol distribution, deposition in the oropharynx was taken as the sum of the activity in the mouth rinse, stomach, and oropharynx after rinsing. Deposition within a region was expressed as a percentage of total deposition.

The adult larynx has been described as an irregular tube, about 4 to 5 cm long, bent anteroposteriorly, which extends from the epiglottal tip to the inferior border of the cricoid cartilage (*7*). In this analysis, laryngeal deposition was defined as the activity detected between the prominence of the thyroid cartilage (the approximate level of the true vocal cords) and the inferior border of the cricoid cartilage. The prominence of the thyroid cartilage was marked using a point source of radioactivity and the marker activity was recorded on the left lateral skull image. The distance between the thyroid cartilage prominence and the inferior border of the cricoid cartilage was measured for each subject and transferred to the deposition images to define the laryngeal region of interest.

## Determination of Intrapulmonary Aerosol Distribution

The anterior image of deposition in the right lung was divided into inner, intermediate, and outer zones by computer. The zones were circular crescents dividing the radius of the right lung into three equal segments. The zones were generated on the xenon ventilation image and aligned with the aerosol image by reference to radioactive point sources taped to the skin during both imaging procedures. The left lung was not used for this analysis because its inner and intermediate zone activities were attenuated by the heart in the anterior view. Counts within each of the three lung zones were divided by the number of pixels in each zone, yielding mean counts/pixel. We assumed that the inner zone contained most of the large airways through the fifth bronchial generation according to Weibel's model (*8*) and that the outer zone consisted almost entirely of peripheral airways under 2 mm internal diameter and alveoli.

## Apex-to-Base Deposition

Deposited activity within apical, intermediate, and basal zones of the right lung was analyzed by computer in a similar fashion. The zones were obtained by

dividing the distance between the highest and lowest points of the right lung into three equal segments. Counts within each zone were divided by the number of pixels in the zone, yielding mean counts/pixel.

## Frequency Distribution Analysis

Frequency distribution histograms were constructed for each aerosol deposition image, with the number of pixels with a given count value expressed as a percent of total lung pixels on the y-axis and the count values on the x-axis. This method of image analysis has been described in detail elsewhere (*9*). The histograms were analyzed for mean counts per pixel, standard deviation, and skew (a dimensionless measure of histogram asymmetry). For this analysis, deposition in the trachea was included with deposition in the lungs.

# Results

The subjects' age, height, and spirometric data are presented in Table 3. Subject 2, the oldest in the group, had an $FEV_1/FVC$ ratio that was borderline normal. He had a history of asthmatic bronchitis approximately 30 years earlier. The bronchitis had remitted entirely and, at the time of this study, he was asymptomatic.

The distribution of aerosol deposition by anatomical division as a percentage of total deposition is presented in Table 4. In subjects 1 and 3, oropharyngeal uptake of the inhaled aerosol equaled or exceeded 95%. In subjects 2 and 4, the oropharynx was a less efficient scrubber: Fractional penetration was greater than 25%.

The intrapulmonary aerosol distribution is shown in Table 5. The ratio of counts per pixel in the inner to outer zone of the right lung (I:O) exceeded 1.0 in the three subjects in whom the analysis was possible (Subject 3 had no detectable lung deposition of radioaerosol). It was more than twice as high in the elderly subject (subject 2) with borderline evidence of airway obstruction as in the two young adults. The Anger camera images of deposition in the intrapulmonary region and trachea of subjects 1 and 2 are shown in Figures 3*A* and 3*B*, respectively.

**Table 5. Intrapulmonary 10-μm aerosol distribution.**

| Subject | Inner: outer zone ratio | Apical: basal zone ratio | Skew[a] |
|---|---|---|---|
| 1 | 2.27 | 0.72 | 1.00 |
| 2 | 4.85 | 0.38 | 1.21 |
| 3 | ND[b] | ND | ND |
| 4 | 1.63 | 1.12 | 0.79 |
| Mean | 2.92 | 0.74 | 1.00 |

[a]Analysis of skew includes trachea.
[b]ND, nondetectable activity.

# Discussion

## Oropharyngeal Deposition

The oropharyngeal deposition efficiency ($DE_O$) in this study ranged from 72 to 99% (Table 4) with the jaw position fixed and no mouthpiece. Predicted $DE_O$ for these conditions, based on a previous study (*10*) in which $DE_O$ was measured during oronasal breathing without recourse to a mouthpiece, ranged from 0.9 to 1.0, although breathing frequency in earlier experiments was lower. Others have studied $DE_O$ during oral breathing through mouthpieces which were 1 to 2 cm in diameter and were held between incisor teeth (*11–14*). Their findings, under different experimental conditions, predict $DE_O$ ranging from 0.1 to 0.75 for the breathing conditions in this study.

**Table 3. Age, height, and spirometric data for male, nonsmoking subjects.**

| Subject number | Age, years | Height, cm | FVC | | $FEV_1$ | | $FEV_1/FVC$, % |
|---|---|---|---|---|---|---|---|
| | | | Observed, L | % Predicted | Observed, L | % Predicted | |
| 1 | 30 | 180 | 7.24 | 134 | 5.50 | 126 | 76 |
| 2 | 66 | 178 | 3.72 | 89 | 2.59 | 79 | 70 |
| 3 | 35 | 183 | 5.79 | 107 | 4.51 | 104 | 78 |
| 4 | 22 | 183 | 5.81 | 109 | 4.68 | 102 | 81 |

**Table 4. Distribution of 10-μm aerosol deposition by anatomical division.**

| | Regional deposition efficiency, as percent of: | | | | | | | |
|---|---|---|---|---|---|---|---|---|
| | Aerosol entering oropharynx | | | | Aerosol entering trachea | | | |
| | Subject number | | | | Subject number | | | |
| Site | 1 | 2 | 3 | 4 | 1 | 2 | 3 | 4 |
| Oropharynx | 95.2 | 74.3 | 99.4 | 72.8 | | | | |
| Larynx | 0.4 | 0.9 | 0.6 | 3.2 | | | | |
| Trachea | 0.4 | 1.5 | ND[a] | 3.3 | 9.1 | 6.0 | ND | 13.8 |
| Lung | 4.0 | 23.3 | ND | 20.7 | 90.9 | 94.0 | ND | 86.3 |

[a]ND, not detected.

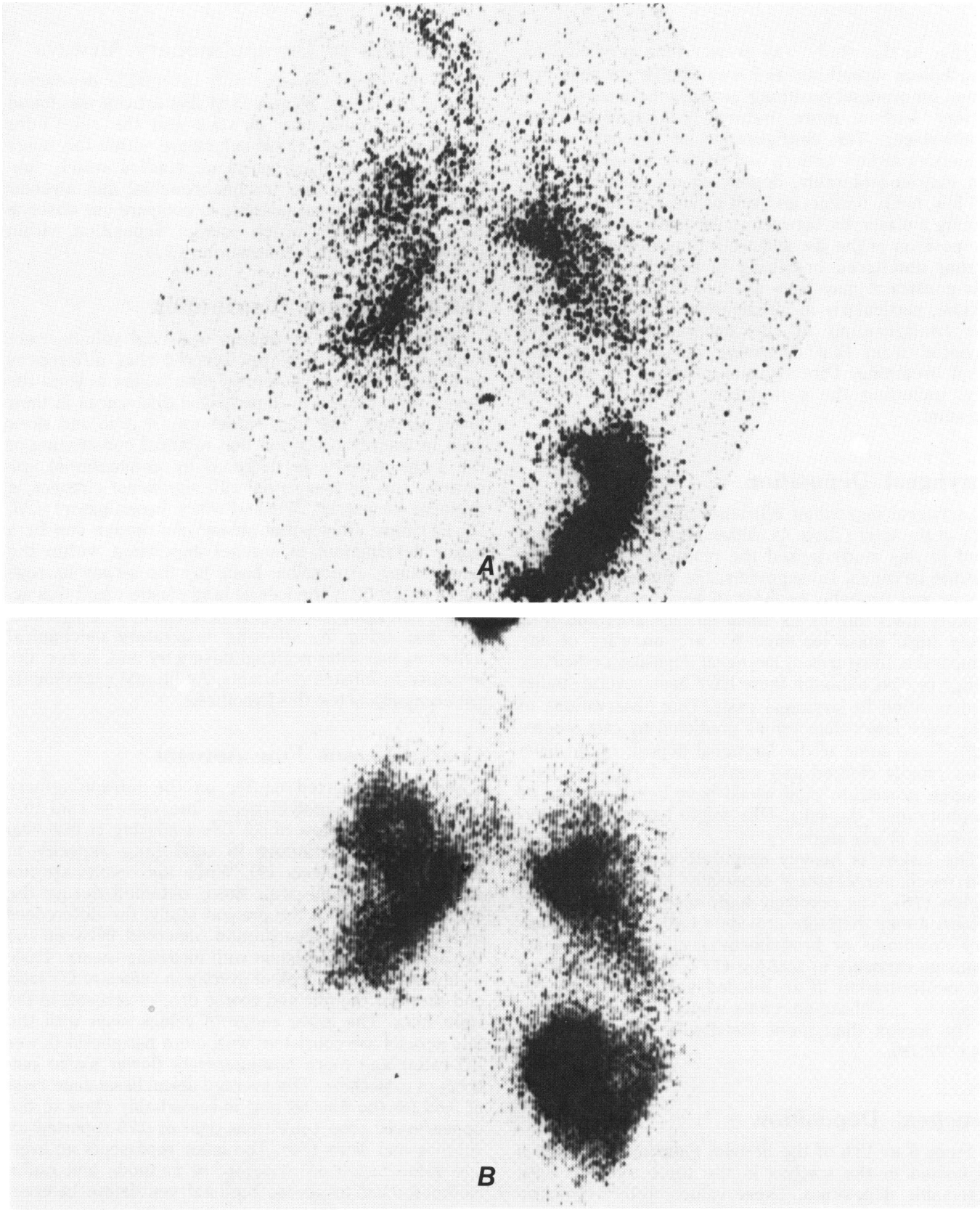


FIGURE 3. Anger camera images (anterior view) of intrathoracic distribution of inhaled 10 μm MMAD $^{99m}$Tc sulfur colloid droplets in (*A*) subject 1 and (*B*) subject 2. Droplets deposited primarily in the trachea and larger bronchi (inner zone) of subject 1, but penetrated to more peripheral airways (outer zone) in subject 2. Due to differences in oropharyngeal filtration efficiency, subject 1 had less aerosol deposition in his lower airways than subject 2. Stomach activity from the swallowed oropharyngeal deposit is visible in the lower right quadrant of each image below the left lung. Laryngeal activity is visible in subject 2 at the top of the image.

$DE_O$ in this study was greater than predicted for mouthpiece breathing and was similar to that predicted for oronasal breathing, probably because the oral airway had a more natural configuration (no mouthpiece). The configuration of the oral airway influences airflow pattern and particle deposition, and can vary considerably, depending on the position of the lips, teeth, tongue, and soft palate. Our rationale for placing a plastic bit between molar teeth was to control the position of the jaw and teeth to positions observed during unfettered breathing in exercise. Insofar as this constraint may have affected the position of the tongue, particularly its relationship to the soft palate, the configuration of the oropharynx may have deviated from that occurring during natural oronasal breathing. Direct visualization of the oropharynx, including the soft palate, could resolve this question.

## Laryngeal Deposition

Laryngeal deposition efficiency ranged from 0.4 to 3.2% of the total (Table 4). Although the Anger camera used in this study lacked the resolution to delineate specific laryngeal subsegments, the tissue dose in the larynx was probably highest of any area of the respiratory tract due to its small surface area and relatively high mass loading. We are unaware of any comparable measures of laryngeal deposition efficiency ($DE_L$) *in vivo*, although there have been several studies of deposition in laryngeal casts. Our observations of $DE_L$ were lower than values predicted by cast studies (*15*). Since some of the laryngeal deposit might have been rapidly cleared and swallowed during the lung imaging procedure (and would have been included as oropharyngeal deposit), $DE_L$ might have been underestimated in our study.

The larynx is heavily endowed with both irritant and mechanoreceptors, especially in the subglottal region (*16*). The relatively high dose to the larynx of subject 4 may therefore provide a basis for the respiratory symptoms or bronchoconstriction that may accompany exposure to acid fog (*17*), particularly since the neutralization of an inhaled acid aerosol by endogenous gas-phase ammonia would be less complete in the larynx than more distally in the respiratory tract (*18,19*).

## Tracheal Deposition

From 6 to 13% of the aerosol entering the trachea deposited in the trachea in the three subjects with detectable deposition. These values were within the range expected based on previous studies *in vivo* (*20*), but were lower than predicted by earlier studies in casts of the larynx and tracheobronchial tree (*15*), assuming a tracheal lumen diameter of 1.7 cm for our subjects.

## Deposition in Intrapulmonary Airways

For the three subjects with detectable deposition beyond the larynx, 86 to 94% of this activity was found in the intrapulmonary airways and the remainder was in the trachea. These values are within the range expected based upon previous studies which subdivided the lung into tracheobronchial and alveolar regions (*14*). It is not possible to compare our observations with models which predict deposition within individual bronchial generations (*21*).

## Intrapulmonary Distribution

Since respiratory frequency and tidal volume were kept constant, it may be inferred that differences among the subjects in aerosol distribution beyond the larynx were related to dimensional differences in their lower airways. The high values for I:0 ratio and skew seen in subject 2 suggest that minimal constriction of the large airways as detected by conventional spirometry can be associated with significant changes in regional dosimetry. We and other investigators (*20, 22–25*) have shown that airway obstruction can be a major determinant of aerosol deposition within the human lung. A possible basis for the airway narrowing in subject 2 is the loss of lung elastic recoil that accompanies aging (*26,27*). It is reasonable to hypothesize that aging, by affecting respiratory mechanical behavior, may alter regional dosimetry and, hence, the response to inhaled pollutants. Additional experiments are necessary to test this hypothesis.

## Coarse Versus Fine Aerosol

We have reported earlier on the intrapulmonary distribution of a polydisperse fine radioaerosol that was inhaled at a flow of 0.5 L/sec starting at 50% vital capacity and continuing to total lung capacity in healthy male subjects (*9*). While the results are not directly comparable with those obtained during the cyclic respiration in the present study, the differences in intrapulmonary distribution observed between the two aerosols are consistent with modeling theory. Table 6 shows a complete lack of overlap in values of I:O ratio and skew for the fine and coarse droplet aerosols in the right lung. The lower range of values seen with the fine aerosol are consistent with more peripheral (lower I:O ratio) and more homogeneous (lower skew) patterns of deposition. The average apical:basal zone ratio of 0.69 for the fine aerosol is remarkably close to the upper/lower zone ventilation ratio of 0.70 reported by Hughes and Amis (*28*). The latter represents an average value based on a variety of methods and radioisotopes used to assess regional ventilation in erect subjects. The apical:basal zone ratio for the coarse aerosol was widely divergent among our three subjects. Of the three vertical subdivisions of the right lung, deposition in the middle portion was greatest for both aerosols (not shown in Table 6).

**Table 6. Intrapulmonary distribution of coarse versus fine aerosol in normal volunteers.**

| Aerosol | $n$ | Inner: outer zone ratio | Apical: basal zone ratio | Skew[a] |
|---|---|---|---|---|
| Coarse[b] | | | | |
| Mean | 3 | 2.92 | 0.74 | 1.00 |
| Range | | 1.63-4.85 | 0.38-1.12 | 0.79-1.21 |
| Fine[c] | | | | |
| Mean | 9 | 1.12 | 0.69 | 0.39 |
| Range | | 0.82-1.30 | 0.59-0.82 | 0.25-0.63 |

[a]Analysis of skew includes trachea.
[b]Coarse, 10 μm MMAD.
[c]Fine, 1 μm MMAD.

## Droplet Stability

We doubt that changes in droplet size occurred following inhalation that would influence deposition site. An inhaled isotonic saline droplet at a relative humidity (RH) of 98% would be expected to increase in mass 10% to reach equilibrium at respiratory tract conditions of 37°C and 99.5% RH (*29*). For a 10 μm droplet, this change in mass would increase particle diameter less than 5%, a change too small to affect the site of deposition. Although the inhaled aerosol was not saturated with water vapor when inhaled (RH = 98%), it is possible that super-saturation could have occurred during inspiration as water diffused into the inhaled bolus of air more quickly than when the bolus was warmed (*29*). The effect of such transient super-saturation on the site of deposition is unknown.

This work was supported in part by grant ES03871 and Center grant ES03819 from the National Institute of Environmental Health Sciences.

### REFERENCES


1. Munger, J. W., Tiller, C., and Hoffmann, M. R. Identification of hydroxymethanesulfonate in fog water. Science 231: 247–249 (1986).
2. American Thoracic Society, Medical Devices Committee (R. M. Gardner, Chairman). ATS Statement—Snowbird workshop on standardization of spirometry. Am. Rev. Respir. Dis. 119: 831–838 (1979).
3. May, K. R. An improved spinning top homogeneous spray apparatus. J. Appl. Phys. 20: 932–938 (1949).
4. Cheah, P. K. P., and Davies, C. N. The spinning-top aerosol generator—improving the performance. J. Aerosol Sci. 15: 741–751 (1984).
5. Niinimaa, V., Cole, P., Mintz, P., and Shephard, R. J. Oronasal distribution of respiratory airflow. Respir. Physiol. 43: 69–75 (1981).
6. Macey, D. J., and Marshall, R. Absolute quantitation of radiotracer uptake in the lungs using a gamma camera. J. Nucl. Med. 23: 731–735 (1982).
7. Geneser, F. Textbook of Histology. Munksgaard Lea and Febinger, Philadelphia, 1986, p. 50.
8. Weibel, E. R. Morphometry of the Human Lung. Academic Press, New York, 1963.
9. Laube, B. L., Links, J. M., Wagner, H. N., Jr., Norman, P. S., Swift, D. L., Koller, D. W., LaFrance, N. D., and Adams, G. K., III. Simplified assessment of fine aerosol distribution in human airways. J. Nucl. Med. 29:1057–1068 (1988).
10. Bowes, S. M., and Swift, D. L. Deposition of inhaled particles in the oral airway during oronasal breathing. Aerosol Sci. Technol. 10: in press.
11. Chan, T. L., and Lippmann, M. Experimental measurements and empirical modelling of the regional deposition of inhaled particles in humans. Am. Ind. Hyg. Assoc. J. 41: 399–409 (1980).
12. Stahlhofen, W., Gebhart, J., and Heyder, J. Experimental determination of the regional deposition of aerosol particles in the human respiratory tract. Am. Ind. Hyg. Assoc. J. 41: 385–398 (1980).
13. Foord, N., Black, A., and Walsh, M. Regional deposition of 2.5–7.5 μm diameter inhaled particles in healthy male non-smokers. J. Aerosol Sci. 9: 343–357 (1978).
14. Lippmann, M. Regional deposition of particles in the human respiratory tract. In: Handbook of Physiology, Section 9: Reactions to Environmental Agents (D. H. K. Lee, H. L. Falk, S. D. Murphy, and S. R. Geiger, Eds.), American Physiological Society, Bethesda, MD, 1977, pp. 213–232.
15. Chan, T. L., Lippmann, M., Cohen, V. R., and Schlesinger, R. B. Effect of electrostatic charges on particle deposition in a hollow cast of the human larynx-tracheobronchial tree. J. Aerosol Sci. 9: 463–468 (1978).
16. Adzakv, F. C. The morphological and functional characteristics of the innervation of the subglottic mucosa of the larynx. Ann. R. Coll. Surg. Engl. 62: 426–431 (1980).
17. Linn, W. S., Avol, E. A., Shamoo, D. A., Anderson, K. R., Whynot, J. R., and Hackney, J. D. Respiratory effects of "acid fog" exposure in normal and asthmatic volunteers. Am. Rev. Respir. Dis. 133: A214 (1986).
18. Larson, T. V. The influence of chemical and physical forms of ambient air acids on airway doses. Environ. Health Perspect. 79: 7–13 (1988).
19. Cocks, A. T., and McElroy, W. J. Modeling studies of the concurrent growth and neutralization of sulfuric acid aerosols under conditions in the human airways. Environ. Res. 35: 79–96 (1984).
20. Lippmann, M., Albert, R. E., and Peterson, H. T., Jr. The regional deposition of inhaled aerosols in man. In: Inhaled Particles III (W. Walton, Ed.), Pergamon Press, London, 1971, pp. 105–122.
21. Gerrity, T. R., Lee, P. S., Hass, F. R., Marinelli, A., Werner, P., and Lourenco, R. V. Calculated deposition of inhaled particles in the airway generations of normal subjects. J. Appl. Physiol. 47: 867–873 (1979).
22. Laube, B. L., Swift, D. L., Wagner, H. N., Jr., Norman, P. S., and Adams, G. K., III. The effect of bronchial obstruction on central airway deposition of a saline aerosol in patients with asthma. Am. Rev. Respir. Dis. 133: 740–743 (1986).
23. Dolovich, M. B., Sanchis, J., Rossman, C., and Newhouse, M. T. Aerosol penetrance: A sensitive index of peripheral airways obstruction. J. Appl. Physiol. 40: 468–471 (1976).
24. Thomson, M. L., and Pavia, D. Particle penetration and clearance in the human lung. Arch. Environ. Health 29: 214–219 (1974).
25. Lin, M. S., and Goodwin, D. A. Pulmonary distribution of an inhaled radioaerosol in obstructive pulmonary disease. Radiology 118: 645–651 (1976).
26. Frank, N. R., Mead, J., and Ferris, B. G., Jr. The mechanical behavior of the lungs in healthy elderly persons. J. Clin. Invest. 36: 1680–1687 (1958).
27. Turner, J. M., Mead, J., and Wohl, M. E. Elasticity of human lungs in relation to age. J. Appl. Physiol. 25: 664–671 (1968).
28. Hughes, J. M. B., and Amis, T. C. Regional ventilation distribution. In: Gas Mixing and Distribution in the Lung (L. A. Engel and M. Paiva, Eds.), Marcel Dekker, New York, 1985, pp. 177–220.
29. Morrow, P. E. Factors determining hygroscopic aerosol deposition in airways. Physiol. Rev. 66: 330–376 (1986).
30. Weathers, K. C., Likens, G. E., Bormann, F. H., Eaton, J. S., Bowden, N. B., Andersen, J. L., Cass, D. A., Galloway, J. N., Keene, W. C., Kimball, K. D., Huth, P., and Smiley, D. A regional acidic cloud/fog water event in the eastern United States. Nature 319: 657–658 (1986).
31. Hoffmann, M. R., Waldman, J. M., Munger, J. W., and Jacob, D. J. The chemistry and physics of acid fogs, clouds, and haze aerosol. In: Aerosols: Research, Risk Assessment and Control Strategies (S. D. Lee, T. Schneider, L. D. Grant, and P. J. Verkerk, Eds.), Lewis Publishers, Chelsea, MI, 1986, pp. 121–149.
32. Pilie, R. J., Mack, E. J., Kocmond, W. C., Eadie, W. J., and Rogers, C. W. The life cycle of valley fog. Part II: Fog microphysics. J. Appl. Meterol. 14: 364–374 (1975).